The Meteoritical Society

Meteoritics & Planetary Science 44, Nr 8, 1193–1202 (2009)
Abstract available online at http://meteoritics.org

Identification of the Bloody Creek structure, a possible impact crater in southwestern Nova Scotia, Canada

Ian SPOONER[1*], George STEVENS[1], Jared MORROW[2], Peir PUFAHL[1], Richard GRIEVE[3], Rob RAESIDE[1], Jean PILON[4], Cliff STANLEY[1], Sandra BARR[1], and David McMULLIN[1]

[1]Department of Earth and Environmental Science, Acadia University, Wolfville, Nova Scotia B4P 2R6, Canada
[2]Department of Geological Sciences, San Diego State University, San Diego, California 92182–1020, USA
[3]Geological Survey of Canada, 601 Booth Street, Ottawa, Ontario K1A 0E8, Canada
[4]Department of Geography, George Mason University, 4400 University Drive, Fairfax, Virginia 22030, USA
[*]Corresponding author. E-mail: ian.spooner@acadiau.ca

(Received 19 January 2009; revision accepted 22 June 2009)

Abstract—An approximately 0.4 km diameter elliptical structure formed in Devonian granite in southwestern Nova Scotia, herein named the Bloody Creek structure (BCS), is identified as a possible impact crater. Evidence for an impact origin is based on integrated geomorphic, geophysical, and petrographic data. A near-continuous geomorphic rim and a 10 m deep crater that is infilled with lacustrine sediments and peat define the BCS. Ground penetrating radar shows that the crater has a depressed inner floor that is sharply ringed by a 1 m high buried scarp. Heterogeneous material under the floor, interpreted as deposits from collapse of the transient cavity walls, is overlain by stratified and faulted lacustrine and wetland sediments.

Alteration features found only in rim rocks include common grain comminution, polymict lithic microbreccias, kink-banded feldspar and biotite, single and multiple sets of closely spaced planar microstructures (PMs) in quartz and feldspar, and quartz mosaicism, rare reduced mineral birefringence, and chlorite showing plastic deformation and flow microtextures. Based on their form and crystallographic orientations, the quartz PMs consist of planar deformation features that document shock-metamorphic pressures ≤25 GPa.

The age of the BCS is not determined. The low depth to diameter ratio of the crater, coupled with anomalously high shock-metamorphic pressures recorded at its exposed rim, may be a result of significant post-impact erosion. Alternatively, impact onto glacier ice during the waning stages of Wisconsinian deglaciation (about 12 ka BP) may have resulted in dissipation of much impact energy into the ice, resulting in the present morphology of the BCS.

INTRODUCTION

In 1987, an approximately 0.4 km in diameter elliptical structure in southwestern Nova Scotia, Canada, was first identified during a regional air photo survey (Stevens 1995). The site is located along Bloody Creek in Annapolis County, approximately 15 km south of Bridgetown (44°45′00″N, 65°14′35″W) at 150 m above sea level (Fig. 1). The Bloody Creek structure (BCS) has a slightly elliptical shape with a 0.42 km long northwest-trending major axis and a 0.35 km long southwest-trending minor axis (Fig. 2). It is defined by a continuous and prominent geomorphic rim that encircles a crater infilled with lacustrine and wetland sediment. A southwest-trending ridge bisects the structure. By the time of the discovery, the site had been flooded as part of the Bloody Creek Reservoir hydroelectric development.

Field investigations of the site were carried out from 1988 until present. Detailed regional air photo and field analyses were carried out to determine the local geological conditions. Ground penetrating radar and magnetic surveys was conducted over the ice-covered reservoir during winter. Bedrock samples for petrographic analyses were obtained from archived collections assembled prior to filling of the reservoir and, more recently, from rim samples retrieved by divers. Notes on the BCS were published by Stevens (1995) and Stevens et al. (2007).

GENERAL GEOLOGY

Regional Geology

The Bloody Creek structure is located in the South Mountain Batholith, an about 388–372 Ma old composite

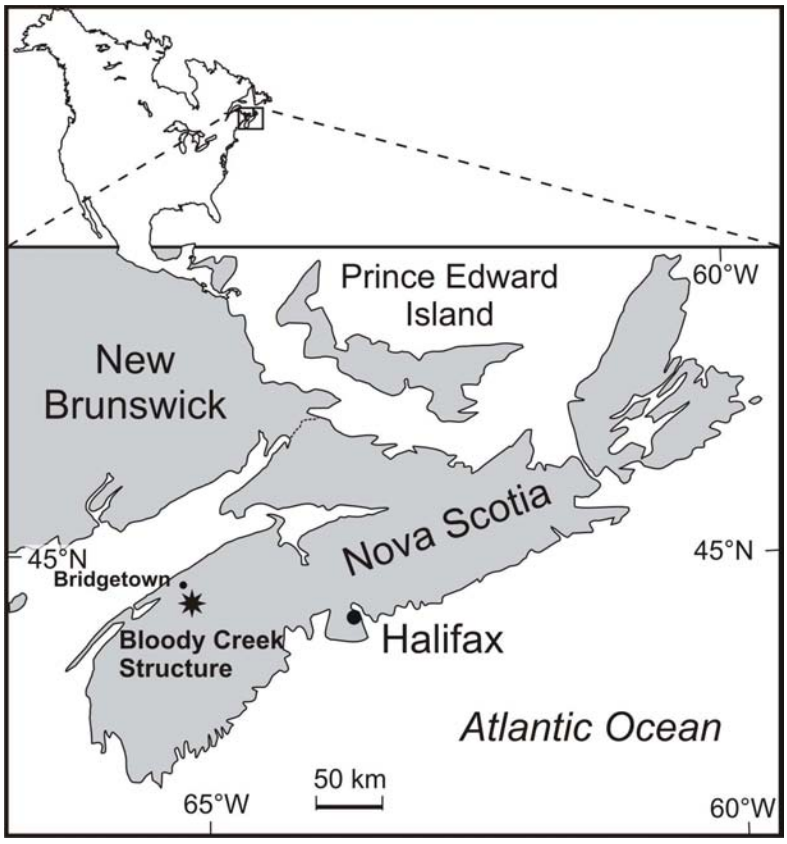

Fig. 1. Location of Bloody Creek structure. The structure is located 15 km south of Bridgetown, Nova Scotia.

granitoid body that underlies about half of southern Nova Scotia (Keppie 2000). The batholith intruded Cambrian to Devonian metasedimentary rocks subsequent to their deformation in the mid-Devonian Neo-Acadian orogeny (Van Staal 2007). The batholith and its host rocks are unconformably overlain by Carboniferous and Triassic-Jurassic rocks of the Maritimes and Fundy basins. Based on texture and composition, the batholith has been subdivided into two groups of plutons, termed Stage 1 (older) and Stage 2 (younger), each of which is relatively homogeneous internally (e.g., MacDonald 1994). The plutons were emplaced at depths of 6–10 km. The Bloody Creek structure is located entirely within the Scrag Lake (Stage 1) Pluton, which consists of medium- to coarse-grained, locally megacrystic, biotite monzogranite.

Surficial Geology

The study area is located within the southwestern portion of the Atlantic Uplands of Nova Scotia as defined by Goldthwait (1924) and is characterized by a gently rolling topography with abundant lakes and marshland. Present landscape morphology and drainage patterns indicate that there were several phases of glacial deposition and that preglacial relief has been largely concealed by recent sedimentary cover. Bedrock exposure is poor due to the low relief and extensive till, lake, wetland and forest cover. The thin (<5 m) till was deposited by local ice caps that were prevalent in Nova Scotia during the last ice age and are characterized by a loose texture, sandy matrix, and abundant, locally derived, angular stones and boulders (Stea and Grant 1982). Where present, the local bedrock has been glacially sculpted and polished. Roche moutonnée and lee side plucking features can also be observed at the site. Relief is low (<10 m) and drainage is poor.

Structure Morphology

The site is located on a fen that was subsequently flooded during reservoir development in the 1990s. Analyses of air photos taken before the site was flooded indicate that the crater has a flat, depressed inner floor that is ringed by a continuous low scarp (1 to 2 m high; Fig. 2). Local bedrock fracture density is highest at the crater rim and decreases outward.

GEOPHYSICS

Ground-Penetrating Radar

Ground-penetrating radar (GPR) surveys were completed in the winter of 1990 when the surface of the

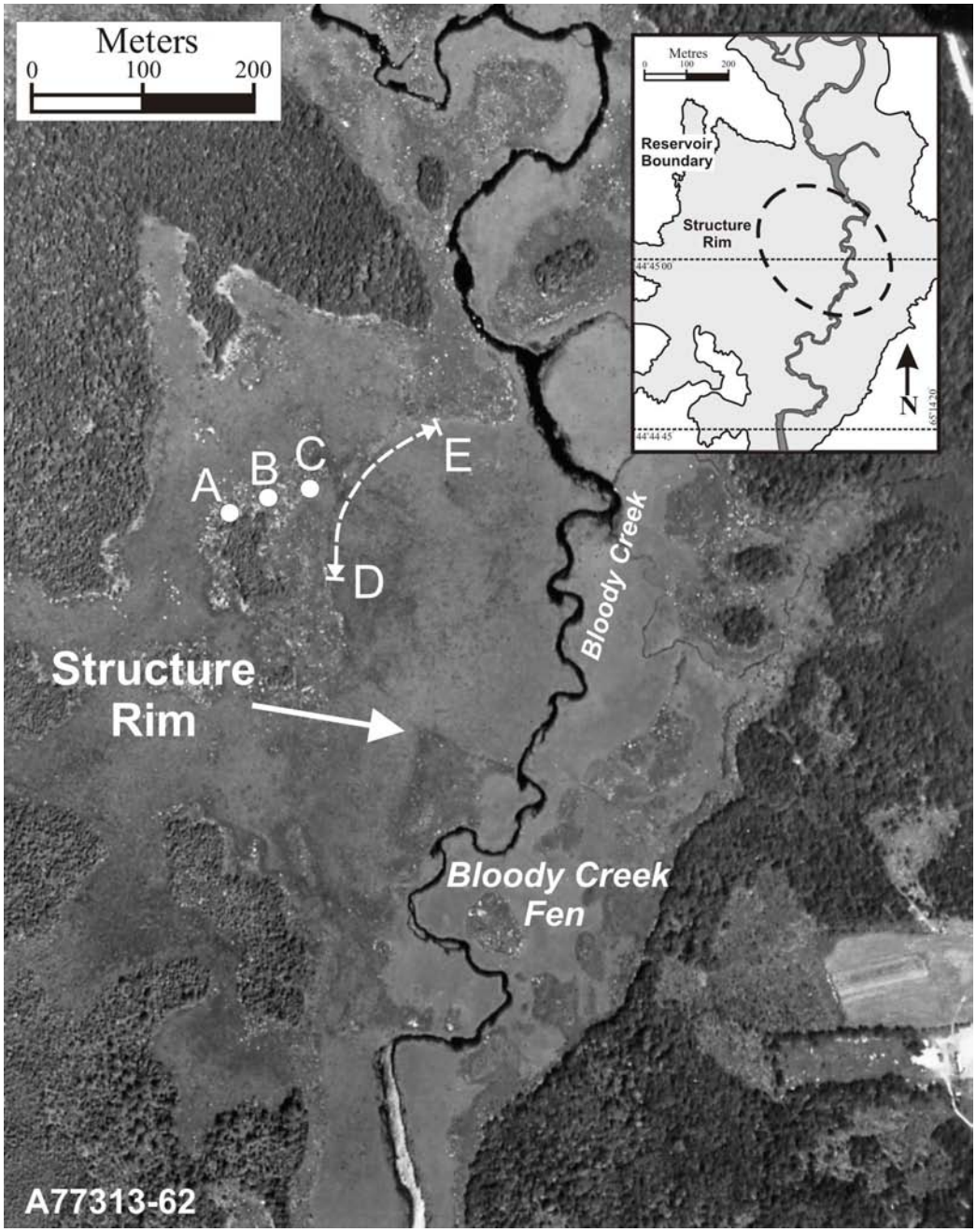

Fig. 2. Aerial photo (A-77313-62) of the Bloody Creek structure. The air photo was taken in July 1977 before the region was flooded for hydroelectric development. The structure is located within a fen flanked by low wooded hills. Thin section sample locations are indicated as A, B, C, and between points D to E. The arrow points to an exposed bedrock outcrop.

reservoir covering the site was frozen. The contrast between electromagnetic properties of ice, water and sediment makes GPR a particularly effective geophysical method for mapping in detail the subsurface structure of the site (Davis and Annan 1989). The surveys were conducted with a bistatic GPR system consisting of a transmitter and receiver connected to a control and data collection console by fiber optic cables. The surveys were conducted at 25 and 50 MHz by attaching the appropriate antennas to the transmitter and receiver units. Data were collected along a total of 6 survey lines that varied in length up to 800 m.

The GPR survey results show the crater-like morphology of the BCS and the distinction of the shallow levels from the undisturbed bedrock (Fig. 3). The core of the BCS appears to be filled with a heterogeneous infill, which clearly exhibit multiple reflections of the electromagnetic (EM) signal because of the very high dielectric contrasts between the ice/water, water/peat and peat/rock interfaces

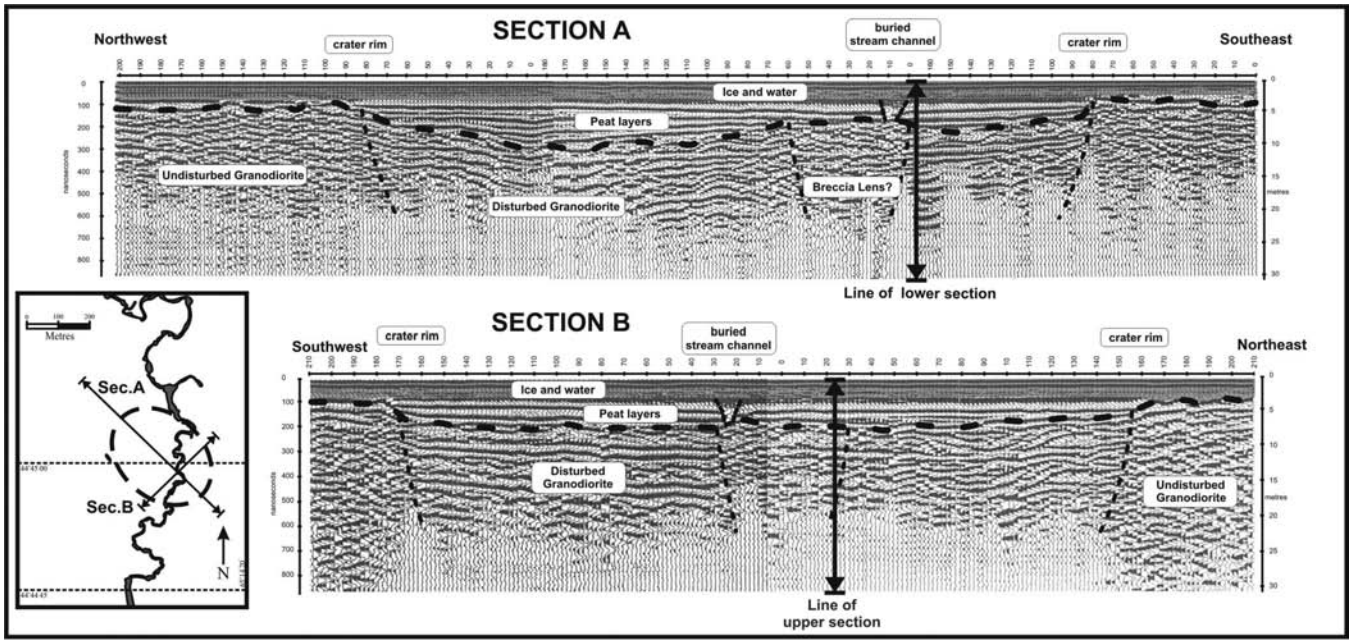

Fig. 3. Ground penetrating radar survey and interpretation of the Bloody Creek structure. Ground-penetrating radar (GPR) traverses were obtained when the site was frozen in winter. They confirm the crater morphology of the structure, and the distinction of the shallow levels from the undisturbed bedrock.

which creates reverberation of the EM signal. These appear as repetitions of the same echoes in time in the profile. These multiple reflections are absent in the GPR profiles of the surrounding country rocks outside of the structure. The infill is separated from the overlying stratified sequence of sediments by an obvious surface of irregular relief. The infilling material is internally faulted as shown by lateral discontinuities in the recorded signals (Fig. 3) and is of uneven thickness, indicating active differential subsidence and compaction.

PETROLOGY

Local Bedrock

Observations on the petrology of the Scrag Lake Pluton rocks are based on (1) a series of 30 representative thin-sectioned samples selected from a large suite of archived bedrock surface samples that were collected during low water conditions along the western shore of the Bloody Creek Reservoir and (2) a set of samples collected at the same time from the submerged structure rim by divers who pried or hammered off pieces of the bedrock. The large suite taken during low water conditions includes samples collected west of, and onto, the western rim crest of the BCS (Fig. 2) This suite documents a progressive increase in probable shock-metamorphic alteration from rim-distal to rim-proximal settings. Thin-section samples were examined optically using both horizontal- and universal-stage (U-stage) petrographic microscopes.

Based on point-count analysis and visual percentage estimates of grains in 10 thin section samples of relatively unaltered bedrock, collected about 90 m northwest of the western rim of the structure (Site A, Fig. 2), the structure is developed in medium- to coarse-grained, hypidiomorphic-granular biotite monzogranite with average mineral modes (by volume) of 31% quartz, 30% plagioclase ($An_{40–50}$), 25% orthoclase feldspar, 10% biotite, 3% muscovite, and 1% accessory minerals. Accessory minerals include, in decreasing relative abundance, ilmenite, apatite, garnet, and zircon. Quartz is generally clear, with sweeping, undulatory extinction, and contains rare to common fluid micro-inclusion trains and irregular, randomly oriented fractures. Both plagioclase and orthoclase feldspars contain common zones altered to sericite (Fig. 4).

Western Rim Rock Alteration Features

Thin-section analysis of 20 samples collected proximal to and on the western rim crest (between points D and E; Fig. 2), supplemented by rim samples more recently collected by divers, document several features that are supportive of shock metamorphism (e.g., Stöffler and Langenhorst 1994; Grieve et al. 1996; French 1998; Langenhorst 2002), including microbrecciation and cataclasis, kink-banding and rare planar microstructures (PMs) in feldspar, reduced mineral birefringence, common mosaicism and PMs in quartz, kink-banding in mica, and systematic degradation of biotite to chlorite showing plastic deformation and flow microtextures (documented in a series

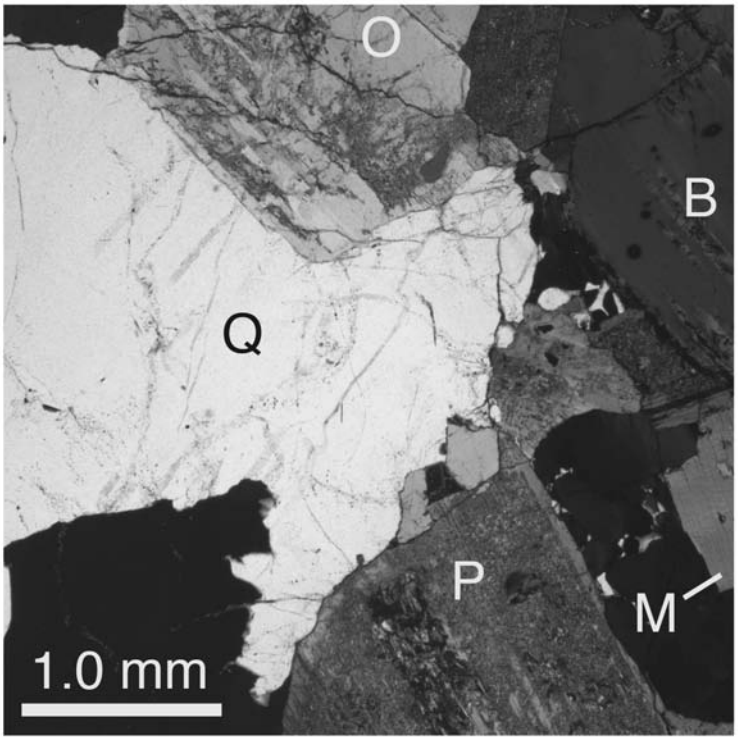

Fig. 4. Thin-section photomicrograph of relatively unaltered bedrock sample collected at surface ~90 m west of western rim of the structure (Fig. 2). Image shows representative mineralogy and microtexture of the bedrock, which is a medium- to coarse-grained monzogranite containing abundant quartz (Q), plagioclase feldspar (P), and orthoclase feldspar (O), and common biotite (B) and muscovite (M). Quartz is generally clear, with sweeping, undulatory extinction, and contains common fluid micro-inclusion trains and irregular, randomly oriented fractures. Patchy, dark, cloudy sericite alteration is common within both feldspar types. Biotite contains common black pleochroic halos around tiny zircon inclusions. Sample 1942-9A (Site A, Fig. 2), cross-polarized light.

of rim-distal to rim-proximal samples). Of these features, single to multiple sets of thin, closely spaced PMs in feldspar and quartz—interpreted as shock-induced planar deformation features (PDFs)—are considered uniquely diagnostic of shock metamorphism (cf. Reimold 2007).

Microbrecciation is common in samples collected on the western rim crest, occurring in anastomozing, polymict lithic breccia veinlets up to several mm across. Locally derived, angular, comminuted feldspar and quartz grains form the microbreccia clasts (Fig. 5A). In some cases, microbreccia clasts can be fitted back into parautochthonous and autochthonous broken mineral grains along the veinlet wall, giving evidence of limited clast transport. The matrix of the microbreccia veinlets consists of finely comminuted mineral grains together with dark, microcrystalline material that is isotropic under cross-polarized light (Fig. 5A inset) and rarely shows apparent flow microtextures. Samples collected on the western rim crest also show extensive alteration of feldspar, including pervasive sericitization, kink-banding (Fig. 5B), and rare, poorly developed PMs. The PMs consist of single sets of thin lamellae, 1–3 μm wide and spaced 4–15 μm apart, which are typically defined by fluid micro-inclusions and oriented oblique to mineral cleavage traces. In addition, apparent reduced birefringence is present in approximately 3 vol% of both feldspar and quartz grains. Reduced birefringence is identified qualitatively in this study on the basis of maximum first order interference color variability in thin section, with consideration given to individual grain orientations and changes in section thickness. Several isotropic feldspar grains were found, indicating a possible very rare occurrence of diaplectic glass.

The most highly altered samples from the western rim crest also contain quartz with abundant fluid micro-inclusions, grain mosaicism under crossed-polarizing light, and common PMs. In contrast to the relatively clear quartz in unaltered bedrock samples collected west of the western rim of the BCS (Fig. 4), quartz in samples at the western rim crest is characterized by a cloudy appearance in plane-polarized light due to the presence of abundant, μm- to sub-μm scale fluid micro-inclusions (Figs. 5C and 5D). Under cross-polarized light, ~50 vol% of the quartz displays an anomalous, mottled extinction pattern that is very unlike the sweeping, undulatory extinction seen in quartz from unaltered samples and most closely resembles shock-induced mosaicism documented in laboratory shock experiments and at numerous proven impact structures (Stöffler and Langenhorst 1994; Grieve et al. 1996; French 1998).

The abundant fluid micro-inclusions in quartz define the

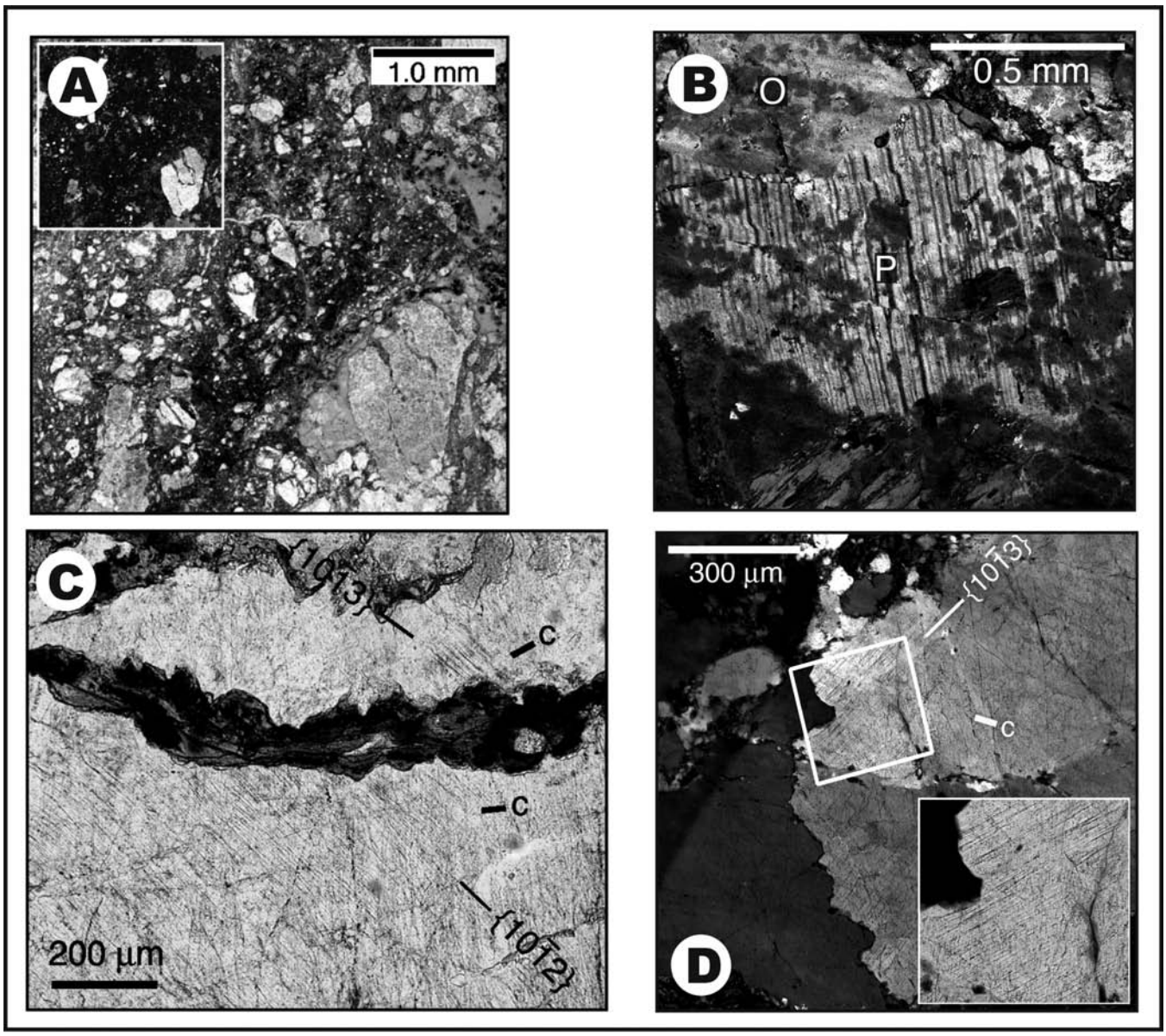

Fig. 5. Thin section photomicrographs of samples collected from rim of BCS, Site D to E, Fig. 2. A) Polymict lithic microbreccia veinlet within probable shocked monzogranite, showing highly comminuted mineral fragments in a dark, microcrystalline, and partly cataclastic matrix. Sample 1974-D, plane polarized light. Inset is reduced view of same image under cross-polarized light, showing isotropic material within matrix. B) Highly altered feldspar in probable shocked monzogranite, including sericite-rich orthoclase (O) and sericite-rich, kink-banded, and micro-fractured plagioclase (P). Mineral at bottom of image, displaying dark, blocky extinction, is chlorite after biotite. Sample 1974-H-6, cross-polarized light. C) Shocked monzogranite showing quartz containing decorated planar microstructures (PMs), including two sets of planar deformation features (PDFs), with Miller indices and c-axes labeled. Quartz grain is cross-cut by veinlet of opaque-inclusion-rich chlorite with possible melt flow microtexture. Sample 1974-H-4, plane-polarized light. D) Shocked monzogranite with quartz containing decorated PMs, including one set of PDFs, with Miller index and c-axis labeled. Inset is enlargement of PDF set. Sample 1974-H-6, cross-polarized light.

occurrence of common, moderately to highly decorated PMs (Figs. 5C and 5D). Under U-stage microscope examination, the quartz PMs consist of one to four sets of planar to slightly curviplanar, inclusion-rich lamellae that are 1–3 μm wide and spaced 4–15 μm apart. The morphology, width, and spacing of these PMs closely matches shock-metamorphic planar fractures (PFs) and PDFs previously described from other documented impact structures (e.g., Stöffler and Langenhorst 1994; Grieve et al. 1996; French 1998). Of these PM sets, approximately one-third have lamellae that are relatively well developed and spaced ≤10 μm apart, representing likely PDFs (Figs. 5C and 5D). These PDFs provide diagnostic evidence of shock-metamorphic conditions associated with formation of the BCS.

Table 1. Summary of planar microstructure (PM) set abundance and indexed PM crystallographic orientations in quartz within monozogranite of Bloody Creek structure rim.

No. of sets:	114
No. of grains:	68
No. of PM sets/grain:	114/68 = 1.7
No. of PM sets/grain; rel% of total grains measured with U-stage microscope	
1 set:	49
2 sets:	38
3 set:	10
4 set:	3
	100
Indexed PM orientations; absolute frequency (%)[a]	
Form:	
c(0001)	5
ω{10$\bar{1}$3}	27
π{10$\bar{1}$2}	25.5
r/*z*{10$\bar{1}$1}	7
ξ{11$\bar{2}$2}	11.5
s{11$\bar{2}$1}	5
x{51$\bar{6}$1}	3
ρ{21$\bar{3}$1}	4.5
Unindexed	11.5
	100

[a]Method described in Engelhardt and Bertsch (1969), Stöffler and Langenhorst (1994), Grieve et al. (1996), and Langenhorst (2002).

A total of 114 PM sets in 68 quartz grains were measured under the U-stage, with an average set abundance of 1.7 sets/grain (Table 1). Grains with one set of lamellae make up 49 vol% of the PM-bearing grains, with two, three, and four lamellae sets present in 38 vol%, 10 vol%, and 3 vol%, respectively, of the remaining grains (Table 1). Indices of the PM crystallographic orientations using the U-stage microscope (method described by Engelhardt and Bertsch, 1969; Stöffler and Langenhorst 1994; Grieve et al. 1996; Langenhorst 2002) indicate that PMs are dominated by plane sets with ω{10$\bar{1}$3}- and π{10$\bar{1}$2}-equivalent crystallographic orientations, which make up 27% and 25.5%, respectively, of the measured sets (Table 1, Fig. 6). In decreasing abundance, other measured PM set orientations include ξ{11$\bar{2}$2}, *r*/*z*{10$\bar{1}$1}, c(0001), *s*{11$\bar{2}$1}, ρ{21$\bar{3}$1}, and *x*{51$\bar{6}$1}. Unindexed PMs make up 11.5% of the measured sets.

Mica is a common component in the bedrock of the BCS, consisting of 10 vol% biotite and 3 vol% muscovite in unaltered monzogranite sampled northwest of the western structure rim. Biotite in unaltered monzogranite is euhedral to subhedral and shows strong pleochroism from tan to dark brown, well-developed {001} cleavage traces, and common black pleochroic halos around tiny zircon inclusions (Fig. 4). Under crossed-polarized light, the biotite shows strong birefringence and characteristic 3rd to 4th order interference colors.

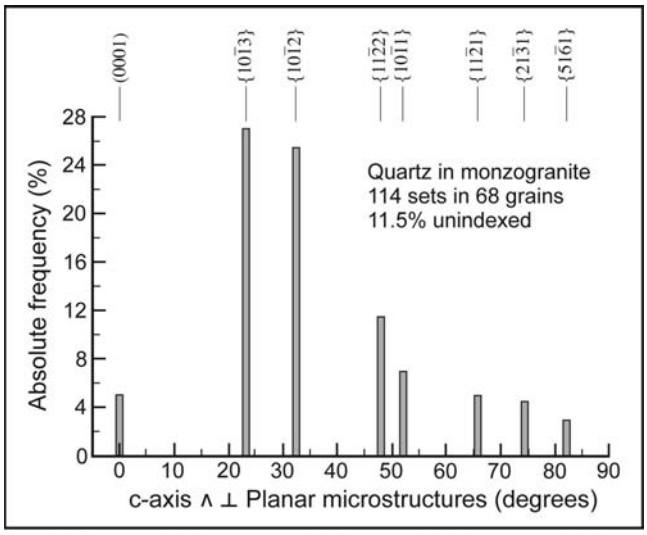

Fig. 6. Histogram of absolute frequency percent of indexed planar microstructures in quartz in monzogranite from the structure rim. Based on 114 sets of planes in 68 grains, with 11.5% sets unindexed (Table 1), measured in samples 1974-H-2, 1974-H-4, 1974-H-5, 1974-H-6, and 1974-H-8 (Site D to E, Fig. 2). Indexing and plotting method after Engelhardt and Bertsch (1969), Stöffler and Langenhorst (1994), Grieve et al. (1996), and Langenhorst (2002).

In a series of thin-section samples examined from west of the BCS towards its western rim crest (Sites B, C, and D to E, Fig. 2), biotite exhibits a progressive, systematic increase in alteration, including partial to total transformation to chlorite, kink-banding, reduction and loss of cleavage traces, reduced birefringence and, locally, isotropization, and development of plastic deformation and flow microtextures (Fig. 7). Under cross-polarized light, the chlorite with plastic deformation and flow microtextures also displays a dark, complex, and blocky extinction pattern characterized by black, isotropic areas intermixed with low-birefringence patches of dark-blue, 1st order interference colors. The systematic alteration of pristine biotite to deformed chlorite towards structure rim parallels the increased development of alteration features in feldspar and quartz, described above. The highest concentration of PMs in quartz coincides with chlorite showing the highest relative abundance of plastic deformation and flow microtextures (Fig. 7D), suggesting that this anomalous alteration of mica is also a by-product of the shock metamorphism.

DISCUSSION

Size and Shape

The BCS is similar in size to the Aouelloul (~390 m, Fudali and Cassidy 1972) and Amguid (~450 m, Lambert et al. 1980) in North Africa. It is, however, morphologically

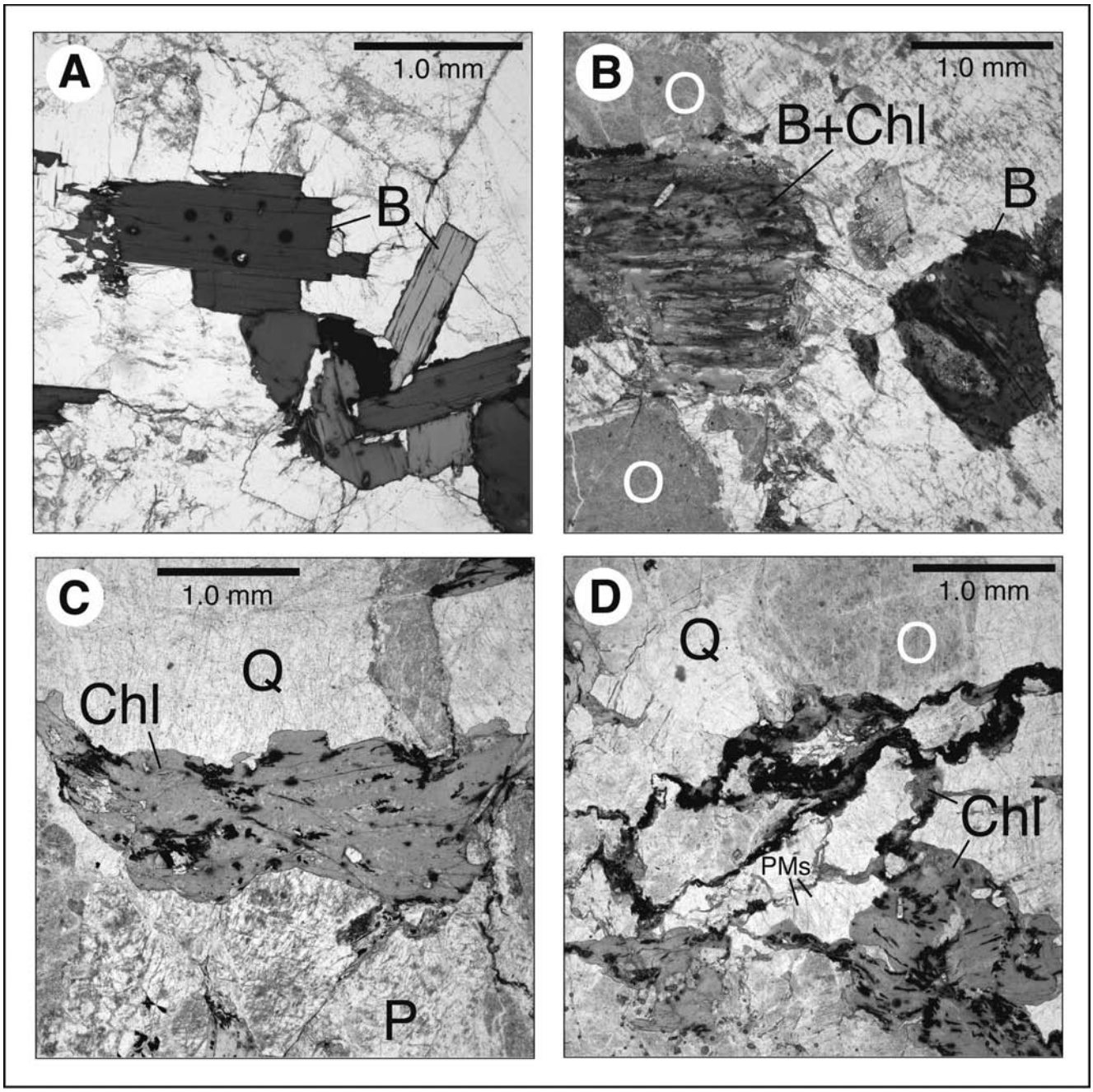

Fig. 7. Thin-section photomicrographs showing progressive increase in mica alteration within representative monzogranite samples collected west of, and on, the western rim of the structure (Fig. 2). All images with plane-polarized light. A) Unaltered biotite (B) laths. Euhedral to subhedral biotite shows strong tan to dark-brown pleochroism, well-developed {001} cleavage traces, and black pleochroic halos around tiny zircon inclusions. Sample 1942-9A, collected ~90 m west of western rim (Site A, Fig. 2). B) Slightly degraded mica laths composed of biotite (B) and mixed biotite and chlorite (B+Chl), co-occurring with sericite-rich orthoclase feldspar (O) and quartz (Q). Mica {001} cleavage traces are present, but poorly developed. Sample 1974-M-1, collected ~50 m west of western rim (Site B, Fig. 2). C) Poorly developed, subhedral to anhedral chlorite (Chl) lath, co-occurring with sericite-rich plagioclase (P) and quartz (Q). Chlorite has rare remnants of cleavage traces and plastic micro-deformation. Common dark inclusions in chlorite are an opaque, ferromagnesian mineral. Quartz is cloudy with mosaic extinction, and contains abundant fluid micro-inclusion trains, some with planar microstructures (PMs). Sample 1948-D-1, collected ~25 m west of western rim (Site C, Fig. 2). D) Distorted, anhedral, opaque-inclusion-rich chlorite (Chl), co-occurring with sericite-rich orthoclase feldspar (O) and quartz (Q). Chlorite shows plastic deformation and interpreted melt flow microtextures into thin veinlets between surrounding fractured silicate minerals (cf. Fig. 5C). Quartz is cloudy with mosaic extinction, and contains abundant fluid micro-inclusion trains, some defining PMs (one example labeled). Sample 1974-H-4, collected from western rim of structure (site between points D and E, Fig. 2).

distinct, as the BCS has an elliptical "rim" with a length to width ratio of 1.2. In addition, it is extremely shallow compared to these structures. Aouelloul and Amguid have outer rim heights above the ground surface of 15–25 m (Koeberl 1994) and up to 50 m (Lambert et al. 1980), respectively. Both of these structures are partially filled with eolian sands and silts. At Aouelloul, gravity and modeling studies suggest an interior depth from the rim to the apparent floor of 23–31 m and a depth of 100–130 m to the base of the underlying breccia lens, i.e., true depth (Fudali and Cassidy 1972; Grieve et al. 1989).

Impacts at very shallow angles result in elliptical impact structures. Laboratory experiments with impacts into non-cohesive sand produced elliptical craters at impact angles of ~5° of the horizontal (Gault and Wedekind 1978). More recent experiments with impact into aluminum targets produced elliptical craters at a steeper impact angle of 12° from the horizontal, which is more in keeping with planetary remote sensing studies and also suggests that there is a target strength effect (Bottke et al. 2000; Herrick and Hessen 2006). The planetary data indicate that ~4% of the crater populations have an aspect ratio of 1.2 or greater. The BCS (420 m × 350 m) has an aspect ratio of 1.2, which is a rarity in the terrestrial impact structure database. The form of the recently discovered 7.5 by 6.3 km (aspect ratio of 1.2) Matt Wilson complex impact structure in Australia has been attributed to oblique impact, based on evidence for up-range to down-range motion in the central structural uplift (Kenkmann and Poelchau 2009). The depths of the transient cavity are reduced in oblique impacts, as is overall cratering efficiency and the degree of shock metamorphism (Pierazzo and Melosh 2000). Thus, if the aspect ratio of the Bloody Creek structure is due to an oblique impact, the relatively high levels of recorded shock pressure in the "rim" require an additional explanation.

Petrology

The co-occurrence of common PDFs in quartz that are dominated by $\omega\{10\bar{1}3\}$ and $\pi\{10\bar{1}2\}$ sets together with other higher index crystallographic orientations (Table 1, Fig. 6) indicates that bedrock exposed at the present rim of the Bloody Creek structure may have experienced shock-metamorphic pressures of up to ~26 GPa (Grieve et al. 1996; Fig. 1). In the nomenclature of Robertson et al. (1968), which is based on a study of progressive shock-metamorphic features observed at 12 Canadian crystalline-target impact craters, the PMs observed at the Bloody Creek structure include the so-called B, C, and D orientations. In this classification scheme, type B quartz includes $\omega\{10\bar{1}3\}$ sets with or without basal c(0001) orientations; type C quartz includes $\omega\{10\bar{1}3\}$ and higher index sets with only rare c(0001) orientations; and type D quartz includes abundant $\pi\{10\bar{1}2\}$ sets, common $\omega\{10\bar{1}3\}$ and higher index sets, no c(0001) sets, and reduced quartz birefringence. Based on shock recovery experiments, the threshold pressure for D features is estimated to be 16 GPa, with a mean pressure of 23 GPa (Robertson and Grieve 1977). These pressure estimates are well above those recorded at the rim of other simple craters and are more in keeping with those recorded in the parautochthonous target rocks at the base of simple craters (Robertson and Grieve 1977). Using the simple, 2.9-km-diameter Brent crater in Ontario, Canada, as a model, the presence of type B, C, and D shocked quartz exposed at the surface would require removal of at least the upper half of the original final crater.

The presence of possible shock-related plastic deformation and flow microtextures in chlorite within the most highly shocked samples (Fig. 7D) is problematic given the maximum estimated shock pressures based on quartz deformation. Using laboratory shock recovery experiments, Schrand and Deutsch (1998) identified degradation and melting of biotite at a pressure of 59 GPa, a pressure level greatly exceeding that indicated by other shock level indicators in our samples. As noted by numerous other studies, however, under conditions of increasing shock pressure, selective, non-equilibrium mineral melting may locally occur first at the interface between different mineral grains (e.g., French 1998). This observation applies to the most highly altered chlorite of this study, which is present at the boundaries between surrounding, less highly shocked feldspar and quartz crystals. Further, the possible very rare occurrence of diaplectic feldspar glass, which is associated with shock pressures of about 35–45 GPa (French 1998), suggests that, at least locally, higher shock levels were reached.

Age of the Structure

The age of the Bloody Creek Crater is indeterminate. The low depth to diameter ratio of the crater structure is anomalous and may be a result of post-impact erosion of the BCS. A possible explanation for the anomalously high threshold pressures indicated by quartz deformation and other alteration features is that the structure is relatively old and has been heavily eroded, presumably, in part by glaciers. What is now observed may be the eroded base of a much larger original structure. This is consistent with the extremely shallow depth-diameter ratio of the structure. Under these conditions the sample sites would have initially been close to the bottom of the original crater. This scenario might also explain why an obvious breccia lens inside the crater is not evident in the GPR data.

The anomalous morphometry of the crater structure may also be a product of impact onto glacial ice. Such a scenario may have resulted in the dissipation of much of the impact energy into the ice, resulting in the low depth to diameter ratio of the crater. Similarities in peat sedimentation rates within

the BCS's crater and in nearby bogs with well-constrained ages indicate that the structure did not form after deglaciation about 12 ka to present (Stea and Mott 1998). However, the peat layers appear to be wedge-shaped and may be faulted, possibly indicating that active differential subsidence and compaction may be continuing, an indication of a relatively young impact structure.

CONCLUSIONS

Petrographic, geophysical and geomorphic evidence indicate that the BCS is likely an impact crater. The elliptical crater rim is not a common feature and may be an indication of oblique impact. The relatively shallow depth of the BCS is anomalous and, together with the high shock-metamorphic pressures recorded at the rim of the crater, may indicate that significant post-impact erosion has taken place. Alternatively, impact onto thin glacier ice overlying bedrock may have resulted in the low relative depth of the BCS.

Acknowledgments–The authors would like thank the Natural Science and Engineering Research Council (NSERC) and the Geological Survey of Canada (contribution 200080731) for funding this research. F. Gillis, B. Hannam, and C. Giffen provided support at the site. We thank K. Milam and J. Ormö for their valuable comments on this manuscript. Thin sections were prepared by Don Osburn, Acadia University.

Editorial Handling—Dr. John Spray

REFERENCES

Bottke W. F., Love S. G., Tytell D., and Glotch T. 2000. Interpreting the elliptical crater populations on Mars, Venus, and the Moon. *Icarus* 145:108–121.

Davis J. L. and Annan A. P. 1989. Ground-penetrating radar for high-resolution mapping of soil and rock stratigraphy. *Geophysical Prospecting* 37:531–551.

Engelhardt W. von and Bertsch W. 1969. Shock induced planar deformation structures in quartz from the Ries crater, Germany. *Contributions to Mineralogy and Petrology* 20:203–234.

French B. M. 1998. *Traces of catastrophe: A handbook of shock-metamorphic effects in terrestrial meteorite impact structures*. LPI Contribution 954. Houston: Lunar and Planetary Institute. 120 p.

Fudali R. F. and Cassidy W. A. 1972. Gravity reconnaissance at three Mauritanian craters of explosive origin. *Meteoritics* 7:51–70.

Gault D. E. and Wedekind J. A. 1978. Experimental studies of oblique impact. Proceedings, 9th Lunar and Planetary Science Conference. pp. 3843–3875.

Goldthwait J. W. 1924. Physiography of Nova Scotia. Geological Survey of Canada Memoir 140. pp. 60–103.

Grieve R. A. F., Garvin J. B., Coderre J. M., and Rupert J. 1989. Test of a geometric model for the modification stage of simple impact crater development. *Meteoritics* 24:83–88.

Grieve R. A. F., Langenhorst F., and Stöffler D. 1996. Shock metamorphism in nature and experiment: II. Significance in geoscience. *Meteoritics & Planetary Science* 31:6–35.

Herrick R. R. and Hessen K. K. 2006. The plan-forms of low-angle impact craters in the northern hemisphere of Mars. *Meteoritics & Planetary Science* 41:1483–1495.

Kenkmann T. and Poelchau M. H. 2009. Low-angle collision with Earth: The elliptical impact crater Matt Wilson, Northern Territory, Australia. *Geology* 37:459–462.

Keppie D. 2000. Geological map of the Province of Nova Scotia. Nova Scotia Department of Natural Resources, Mines and Energy Branch, Map ME2000-1, scale 1:500,000.

Koeberl C. 1994. African meteorite impact craters: Characteristics and geological importance. *Journal of African Earth Science* 18: 263–295.

Lambert P., McHone J. F. Jr., Dietz R. S., and Houfani M. 1980. Impact and impact-like structures in Algeria. Part 1. Four bowl-shaped depressions. *Meteoritics* 15:157–179.

Langenhorst F. 2002. Shock metamorphism of some minerals: Basic introduction and microstructural observations. *Bulletin of the Czech Geological Survey* 77:265–282.

MacDonald M. A., ed. 1994. Geological map of the South Mountain Batholith. Nova Scotia Department of Natural Resources, Mines and Energy Branch, Map 94–01, scale 1:250,000.

Pierazzo E. and Melosh H. J. 2000. Understanding oblique impacts from experiments, observations and modeling. *Annual Review of Earth and Planetary Sciences* 28:141–167.

Reimold W. U. 2007. The Impact Crater Bandwagon (Some problems with the terrestrial impact cratering record). *Meteoritics & Planetary Science* 42:1467–1472.

Robertson P. B., Dence M. R., and Vos M. A. 1968. Deformation in rock-forming minerals from Canadian craters. In *Shock metamorphism of natural materials*, edited by French B. M. and Short N. M. Baltimore: Mono Book Corporation. pp. 433–452.

Robertson P. B. and Grieve R. A. F. 1977. Shock attenuation at terrestrial impact structures. In *Impact and explosion cratering*, edited by Roddy D. J., Pepin R. O., and Merrill R. B. New York: Pergamon Press. pp. 687–702.

Schrand C. and Deutsch A. 1998. Formation of lechatelierite and impact melt glasses in experimentally shocked rocks (abstract #1671). 29th Lunar and Planetary Science Conference. CD-ROM.

Stea R. R. and Grant D. R. 1982. Pleistocene geology and till geochemistry of southwestern Nova Scotia (Sheets 7 and 8). Nova Scotia Department Mines and Energy Map 82–10.

Stea R. R. and Mott R. J. 1998. Deglaciation of Nova Scotia: Stratigraphy and chronology of lake sediment cores and buried organic sections. *Géog Phys et Quat* 52:1–19

Stevens G. R. 1995. Meteor Crater, Nova Scotia. *The Journal of the Royal Astronomical Society of Canada* 89:111–113.

Stevens G. R., Spooner I. S., Morrow J. R., Pufahl P., Raeside R., Grieve R. A. F., Stanley C., Barr S., and McMullin D. 2007. Physical evidence of a late-glacial (Younger Dryas?) impact event in southwestern Nova Scotia (abstract U23A-0854). *Eos Transactions*, American Geophysical Union, Fall Meeting Supplement 88(52).

Stöffler D. and Langenhorst F. 1994. Shock metamorphism of quartz in nature and experiment: I. Basic observation and theory. *Meteoritics* 29:155–181.

Van Staal C. R. 2007. Pre-Carboniferous tectonic evolution and metallogeny of the Canadian Appalachians. In *Mineral deposits of Canada: A synthesis of major deposit-types, district metallogeny, the evolution of geological provinces, and exploration methods*, edited by Goodfellow W. D. Geological Association of Canada, Mineral Deposits Division, Special Publication No. 5. pp. 793–818.